Experimental study of the effect of wing sweep on transonic buffet

D'Aguanno, A.; Camps Pons, C.; Schrijer, F.F.J.; van Oudheusden, B.W.

DOI
10.2514/6.2022-1807

Publication date
2022

Document Version
Final published version

Published in
AIAA SCITECH 2022 Forum

AIAA SciTech Forum
January 3-7, 2022, San Diego, CA & Virtual
AIAA SCITECH 2022 Forum

10.2514/6.2022-1807

Experimental study of the effect of wing sweep on transonic buffet

A. D'Aguanno[1]*, C. Camps Pons[1], F.F.J. Schrijer[1] and B.W. van Oudheusden[1]

[1]: *Aerodynamics Sect. (AWEP), Delft University of Technology, 2629 HS Delft, The Netherlands*

** Corresponding author: A.Daguanno@tudelft.nl*

In this study the effect of wing sweep on transonic buffet is studied experimentally to reveal the differences between two-dimensional (2D) and three-dimensional (3D) wing configurations. Background oriented schlieren (BOS) and stereographic particle image velocimetry (PIV) have been used as measurement techniques, performing experiments on: an airfoil, an unswept wing and two swept wings with a sweep angle of 15° and 30° respectively (all wings are based on the OAT15A airfoil). All wings have been tested at a constant normal Mach number ($Ma_{\infty n}$=0.7) with respect to the leading edge. The results show that the buffet oscillations are much stronger for the airfoil than for the three finite-span wings. A large difference in the buffet behavior can be noticed between the airfoil and the unswept wing, particularly in correspondence of the more outboard spanwise locations, suggesting that in the latter an important role could be played by finite-wing effects, notably the tip vortex. A spectral analysis has shown that for the swept wings the classical 2D buffet peak (occurring at f=160 Hz for the present conditions) is substantially attenuated, while additional contributions in the range of 450-850 Hz appear. The PIV results showed, for the 30° sweep angle wing, a periodical occurrence of a secondary supersonic area downstream of the main shockwave structure, which is absent for the other wing models. The stereographic PIV configuration allowed the reconstruction of the spanwise oriented velocity component, obtaining in the trailing edge area, spanwise outboard velocities (80-100 m/s) which are in agreement with the spanwise convection of buffet cells observed in literature in this region.

I. Introduction

The flight envelope of civil aircraft is limited by the onset of transonic buffet. This phenomenon consists in the oscillation of a shockwave on the suction side of the wing, which occurs for a specific range of angle of attack (α), Mach (Ma) and Reynolds number (Re). These oscillations could eventually result in failure of the wing due to fatigue as well as to unsteadiness in the aerodynamic characteristics.

The occurrence of transonic wing buffet has been extensively studied in the last 30 years, notwithstanding that first studies have already been undertaken as early as 1952 by Ref. [1]. This phenomenon has been explained in 1990 by Ref. [2] as the result of a feedback mechanism, with the shockwave (SW) oscillation being sustained by the presence of downstream propagating vortical structures, which travel from the shock foot towards the trailing edge area, and by upstream traveling pressure waves (i.e. UTWs induced by the presence of the vortical structures) which moving in the direction of the shockwave, according to the buffet phase, allow the SW to move either downstream or upstream. This physical model has been subsequently updated by different researchers, such as Ref. [3, 4], who considered the UTWs capable of reaching the SW, along both the suction and the pressure side of the airfoil. Recently, a dedicated study undertaken by Ref. [5] clarified that the UTWs are acoustic waves which propagate with a velocity of 80 m/s, relative to the flow. A further investigation of Ref. [6] has given hints that the UTWs are produced during the entire buffet cycle, albeit with a modulated strength depending on the buffet cycle phase.

A crucial contribution to the understanding of transonic two-dimensional (2D) buffet has been given by Ref. [7], who described transonic buffet as the result of a modal instability, obtaining values for the buffet onset conditions which

are in perfect agreement with experimental observations. Similar results were also obtained by the stability analysis of Ref. [8].

All the previous studies were conducted on airfoils, corresponding to unswept, infinite-wing conditions, while more dedicated research on swept wings has been pursued only in more recent years. The study of buffet on swept wings is very relevant because of its possible occurrence in real flight conditions and actual wing configurations, however, a complete comprehension of the phenomenon is still far from being achieved. In presence of wing sweep, the buffet mechanism appears to be much more complicated, with oscillations of the shockwave in the chordwise direction being of lower amplitude [9] compared to the airfoil case and occurring at much higher frequencies. For swept wings the typical 2D isolated peak at St=0.07 is substituted by a broadband peak in the range of $0.2<St<0.6$, with St being the Strouhal number based on the free stream velocity and the chord of the wing ($St=f\cdot c/U_\infty$). From recent experiments by Ref. [10] on a 30° swept wing based on the OAT15A airfoil, a buffet onset of Ma=0.82 at $\alpha=3°$ is obtained. It should be noticed that the angle of attack has an important influence as well, inducing either simultaneous 2D and three-dimensional (3D) shock-buffet behaviors, or only 3D behavior, depending on the trailing edge separation characteristics [11]. The simultaneous presence of these two behaviors is also confirmed by a modal decomposition (of a zonal detached eddy-simulation) on a wing-body configuration [12].

Ref. [13] described the flow pattern of a 30° swept wing based on the OAT15A airfoil section, resulting in a normal shockwave and a quasi-2D flow for outboard locations, and a λ shock and highly 3D flow for inboard locations.

Ref. [14] studied the effect of the sweep angle, obtaining that for infinite wings with sweep angles larger than 20° the difference in behavior with respect to 2D models is very relevant. In contrast, for sweep angles $\Lambda<20°$ no substantial difference is observed. The main cause for this difference is associated with the spanwise convection of particular flow structures that occurs at high sweep angles, which is referred to in Ref. [14] as buffet cells. The buffet cells consist in pressure disturbances of alternating sign, which are periodically convected from the wing root (aft of the λ shock) towards the wing tip.

The presence of buffet cells is also confirmed by different experimental studies such as Ref. [9-11]. In Ref. [9], different experimental databases, belonging to four projects (BUFET'N Co, AVERT, DTP and FLIRET) are compared. The different datasets are all based on wings with a sweep angle of 30° and they all show the presence of a spanwise convection velocity equal to $0.25\cdot U_\infty$ proceeding outboard in the shockwave oscillation range. In addition to the previous convection phenomenon, another spanwise convection velocity of 100 m/s ($0.36\cdot U_\infty$) is observed in the separated area, with similar results also obtained by Ref. [15]. Convection phenomena are also detected in the chordwise plane and attributed to K-H instability (with typical propagation velocity of $0.65\cdot U_\infty$). A discussion of the origin of the buffet cells is also given in Ref. [16], where the buffet cells are described as reminiscent of the stall cells observed in low speed conditions.

Ref. [14] has also addressed the finite wing effect, showing that for a finite swept wing, end-effects and wall interference are present. These effects cause the formation of tip vortices, which influence the transonic buffet behavior in the more outboard sections [14], while recovering the infinite swept wing behavior in the more inboard sections. These results are also confirmed by the numerical study of Ref. [17].

In contrast, finite-wing effects on transonic buffet in connection to unswept wings has received relatively little attention in literature and requires further research. Nevertheless, some studies have been conducted on the confinement effects on airfoils (therefore in absence of free wing tip), such as in the numerical study of Ref. [18], where differences in the airfoil performance are noted when modelling top, bottom and side walls of the wind tunnel. Ref. [3] by analyzing oil flow visualization results, commented that possible 3D side wall effects are contained in proximity of the two extremities of the airfoil model.

Besides the physical description given by Ref. [14], Ref. [19] has also described three-dimensional buffet applying stability analysis to both swept and unswept infinite wings. In presence of wing sweep, spatial modes were found to become unsteady, propagating periodic flow structures towards the wingtip, in good agreement with existing literature. For an unswept wing, these spatial modes are still present although steady, in addition to the classical 2D buffet mode. This analysis has also been extended by Ref. [20] to finite wings.

It should be considered that the experimental swept-wing models investigated in literature, as in the experimental database discussed by Ref. [9], differ from 2D buffet models not only for the presence of the sweep angle, but also for the taper ratio and the presence of a fuselage. Therefore, it is difficult to isolate the effect of the sweep angle in transonic buffet. To achieve this goal in the current study, wings with different sweep angles and with constant chord have been studied and compared to the behavior of an airfoil that fully spans the wind tunnel test section, in order to quantify both sweep and tip effects.

Most of the experimental studies present in literature make use of pressure measurements on the suction side of the wing employing either unsteady pressure transducers [9, 10, 21] or pressure sensitive paint [11, 22, 23]. In this paper the main investigation is conducted by using stereo-particle image velocimetry, for reconstructing the three velocity

components in several planes of measurement oriented along the free stream direction, at different spanwise locations. The use of PIV is not uncommon in the study of transonic buffet on airfoils (see for example [5, 24, 25]), however, to the best of the authors' knowledge no previous study has considered PIV to study transonic buffet on swept wings. The application of PIV could help to visualize and analyze the main flow structures characterizing transonic buffet on swept wings, which is not always allowed with wall pressure measurements.
In addition to PIV, the background oriented schlieren (BOS) technique has been used to provide a further characterization of the flow field,. BOS was already successfully adopted in Ref. [6] for the study of transonic buffet on a 2D airfoil, but its application in this intrinsically three-dimensional application has not been demonstrated yet and will be tested by comparing the results with PIV.

II. Experimental investigation

A. Facility and flow conditions

The current experimental study has been performed in the transonic-supersonic wind tunnel (TST-27) of TU Delft, which is a blowdown wind tunnel with a test section 25.5 cm high and 28 cm wide. The experiments have been carried out with a total pressure p_0=2 bars, total temperature T_0=288 K and with the free stream Mach number in the range Ma_∞=0.70-0.81. The variation of the transonic Mach number is achieved by adjusting a throat located downstream of the test section, allowing an accuracy of Ma to the third decimal digit to be achieved. The values of the main flow conditions are reported in Table 1.

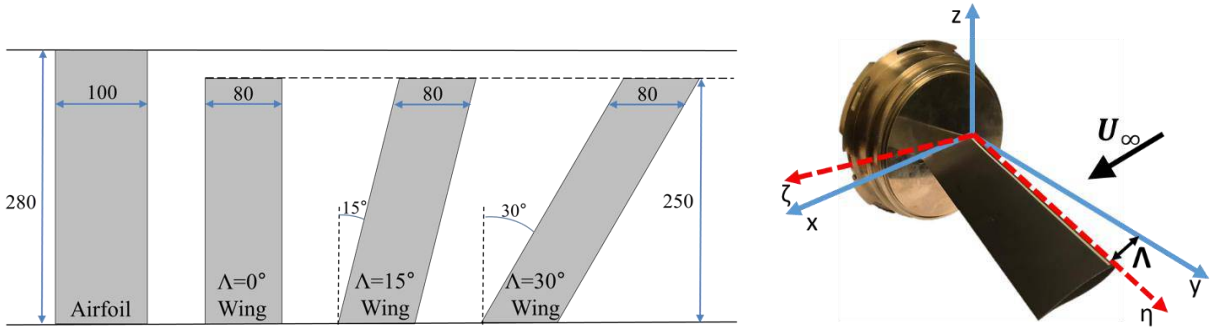

Fig. 1 Sketch of the models based on the OAT15A airfoil (left) with dimensions in mm and angles in degrees. On the right, the 15° sweep angle model attached to the clamping piece with indication of the two coordinate systems used.

B. Wing models

The models used for the experiments are wings obtained from the extrusion of an OAT15A airfoil with three different sweep angles, Λ=0°, Λ =15° and Λ =30°, a chord (c) of 8 cm and a span (b) of 25 cm. The choice of the airfoil (OAT15A) and the values of the sweep angle are motivated by similar studies present in literature (see [9, 26]). The wings are clamped at the root to one of the side walls, with optical access provided from the opposite side of the test section. In addition to the three wings, an airfoil having a chord of 10 cm and a span of 28 cm (clamped at both sides of the wind tunnel) has been tested as well. This model has been extensively studied in the same wind tunnel for buffet applications in previous experiments [24]. For the finite-span wings, the distance of the wing tip to the side windows (3 cm) has been chosen to ensure that the wing was not immersed in the turbulent boundary layer developing on the side wall of the test section.

Table 1 Flow conditions (normal with respect to leading edge).

Parameter	Symbol	Value
Free stream normal Mach number	$Ma_{\infty n}$	0.7
Free stream normal velocity	$U_{\infty n}$	225 m/s
Total temperature	T_0	288 K
Total pressure	p_0	2 bar
Reynolds number per unit length	Re/L	$2.6 \cdot 10^7$ 1/m

A sketch of the top view of the different wing models is shown in Fig. 1 (left), with the main geometric characteristics included. In Fig. 1 (right) the 15° swept wing is shown together with the clamping piece by which the models are mounted to the wind tunnel side wall. Similar as in other studies [3, 5] a transition trip has been applied to all the models at 7% c to ensure a turbulent boundary layer. The trip has been realized with Carborandum 500 particles, as in Ref. [24].

For the airfoil the most developed buffet condition is obtained for Ma=0.7 and α=3.5°, as shown in a previous experimental study [24] in the same wind tunnel. Correcting the Mach number for blockage effects, a value of Ma=0.73 is achieved, which is in good agreement with the value found by Ref. [3] for the same airfoil.

In this study the different wings are tested with the same value of the normal Mach number with respect to the leading edge ($Ma_{\infty n}$=0.7). The values of the free stream Mach number and angle of attack used for each model are summarized in Table 2, together with the respective geometric parameters (chord and span).

Table 2 Flow and geometric properties of the models

Model	Ma_∞ (-)	α (°)	c (m)	b (m)
Airfoil	0.7	3.5	0.10	0.28
Λ=0° wing	0.7	3.5	0.08	0.25
Λ=15° wing	0.72	3.4	0.08	0.25
Λ=30° wing	0.81	3.4	0.08	0.25

C. Experimental set-up

The experiments have been conducted using two different optical techniques, background oriented schlieren (BOS) and particle image velocimetry (PIV). BOS has been selected instead of schlieren because for the three finite wings the optical access was possible only from one side of the wind tunnel. The set-up used for the BOS experiments consists of a LED lamp for illumination and a high speed recording camera directly looking at the speckle pattern, the latter being attached to the clamping piece at the wing root. A sketch of the BOS set-up in top view is shown in Fig. 2 (left). A LaVision Imager Pro HS4 camera is used with an acquisition frequency of 4.65 kHz which allows to resolve the shock oscillation in time. To reach that acquisition frequency, the resolution of the camera has been cropped to 1008×468 pixels, acquiring 4000 images per wind tunnel test. By using a 105 mm lens a field of view (FOV) including the entire chord of the models has been obtained, as indicated in Fig. 2 (right).

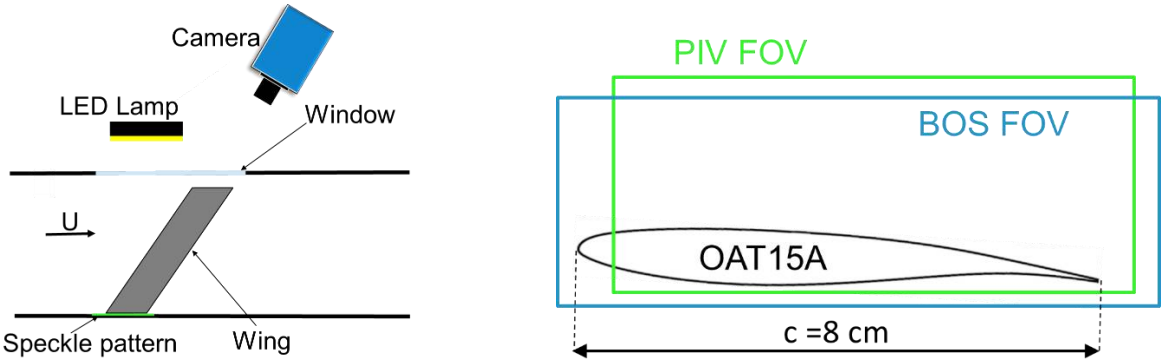

Fig. 2 Top view of BOS set-up (left). On the right the BOS and PIV FOVs.

The speckle pattern has been realized with black dots on a white background. An example of the speckle pattern used is given for the unswept wing in Fig. 3 (left), with clear compressibility effects revealed in the area where the speckle pattern is deformed. The region in which high compressibility effects are evident is not a line, as it should be in presence of a normal shockwave at a given spanwise position. The reason for this is associated with the integration of the variable density gradient along the span of the wing/airfoil. In order to minimize the 3D effects in the BOS images the viewing direction of the camera has been aligned along the leading edge of the different wings, as also sketched in Fig. 2 (left).

To quantitatively investigate the flow field, stereo-PIV tests have been performed, using the set-up shown in Fig. 4 (left). Two high speed cameras (Photron Fastcam SA1.1) in stereo configuration with an acquisition frequency of 4.65 kHz and in double pulse mode (pulse separation Δt=3μs) have been used for acquiring images for a total time duration of t=0.94 s (4365 pairs of images per camera). In order to achieve the selected acquisition frequency the sensor of the cameras has been cropped to 1024×640 pixels. Both cameras have been equipped with lenses with a focal length of

105 mm and an f-stop $f_{\#}$=8; in addition, two Scheimpflug adaptors have been used to align the focal plane with the image plane (laser plane). These settings resulted in a field of view in the chordwise plane which is 8 cm long and 5 cm high (12 pix/mm) as sketched in Fig. 2 (right). Limitations in the optical access have constrained the angle between the cameras to approximately 60°. The use of the stereo configuration allows the determination of the out-of-plane velocity component, which is of crucial importance to characterize a 3D flow.

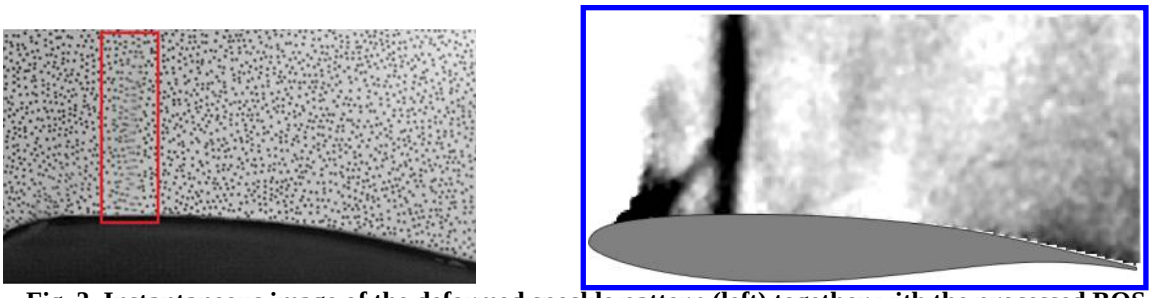

Fig. 3 Instantaneous image of the deformed speckle pattern (left) together with the processed BOS image, which displays the horizontal displacement of the speckle pattern (right).

The seeding particles used are DEHS (Di-Ethyl-Hexyl-Sebacat), which have a relaxation time of 2μs (see Ref. [27]). In view of their relaxation time, the particles are not able to faithfully follow the flow in regions of strong flow deceleration, as notably occurring for shockwaves. Therefore, in such flow regions, the velocity measurement is affected by a particle slip uncertainty (ε_{slip}=50 m/s across the shockwave).
The particles are illuminated by a high speed dual cavity Mesa PIV laser (Nd:YAG), forming a light sheet of 1.5 mm thickness. The laser illumination was synchronized with the cameras using a LaVision high speed controller (art. 1108075). The laser beam is introduced in the test section by means of a laser probe entering from one of the side walls of the wind tunnel (see Fig. 4 (left)). By simultaneously sliding the laser probe and the cameras, tests at different span locations have been performed, in particular at y/b=0.4, 0.5, 0.6 and 0.7 for the unswept wing and at y/b=0.5, 0.6 and 0.7 for the remaining two wings, as indicated in Fig. 4 (right).

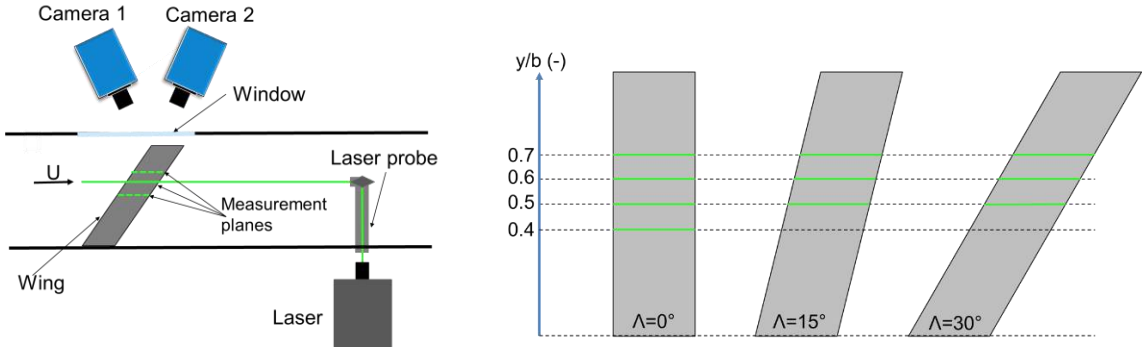

Fig. 4 Stereo-PIV set-up (left) and location of the PIV planes of measurement (right).

D. Data processing

Both the BOS and the PIV images were collected and partly processed in LaVision Davis 10.0.5. For the BOS images, each instantaneous snapshot of the speckle pattern in presence of density gradients was cross-correlated with a reference image (obtained with the wind tunnel off). A multi pass approach with an initial window size of 32×32 pixels and a final window size of 16×16 pixels and an overlap of 75% was applied, reaching a final vector spacing of 0.028 cm (corresponding to 0.28% c for the airfoil and 0.35% c for the wings). In Fig. 3 (right) an example of a BOS processed image is shown, resulting from a cross-correlation of the raw image in Fig. 3 (left) with the reference no-flow image. This processed image clearly quantifies the deformation of the pattern due to the (density) compressibility effects, and as such visualizes the near-normal shockwave as well as the oblique Mach wave originating from the transition trip.
For the PIV images, to reduce the laser reflections from the model, a minimum subtraction has been used by means of a Butterworth filter with a filter length of seven snapshots (see for more details Ref. [28]). Subsequently a stereo cross-correlation procedure was performed, using again a multi-pass approach with an initial window size of 96×96

pixels and a final window size of 32×32 pixels and an overlap of 75%. These settings resulted in a vector spacing of 0.82%c. The vector uncertainty associated to the cross-correlation procedure can be computed similarly for BOS and PIV, as described by Ref. [29]. The associated value is lower than 0.1 pix and therefore leads to an uncertainty in the PIV velocity evaluation of 6.67 m/s. In Table 3 the main PIV and BOS settings and corresponding uncertainties are summarized. Further processing for both BOS and PIV data has been carried out in Matlab.

Table 3 BOS and PIV settings and uncertainties

Parameter	BOS	PIV
Acquisition frequency	4.65 kHz	4.65 kHz
Number of images	4000	4365
Final image resolution	1008×468 pix	1024×640 pix
Final window size	16×16 pix	32×32 pix
Window overlap	75%	75%
Vector spacing	0.28%c (airfoil) - 0.35%c (wings)	0.82% c
Cross-correlation uncertainty	<0.1 pix	<6.67 m/s
Particle slip	N.A.	<50 m/s (in shock areas)

III. Comparison of airfoil and unswept wing behavior

A. Shock dynamics comparison by means of BOS

Although there are many studies in literature which describe the transonic buffet behavior on airfoils, there is no study where a comparison between the performance of an airfoil and an unswept wing of finite span is addressed. In this study these two aspects are directly compared, using the BOS results on the two models at the same flow conditions (Ma=0.7 and α=3.5°).

The shock position has been tracked for both configurations, as extracted from the gradient of the density field. The variation of the shock position in time is shown in Fig 5 (left). It is evident that the shockwave is located much more upstream for the unswept wing (the mean shock position for the unswept wing is $X_{SW\ AVG}$= 28.3% of the chord, while for the airfoil this is $X_{SW\ AVG}$=42.8% c) and that the amplitude of oscillation is larger for the airfoil. This is confirmed by the standard deviation (STD) of the shock position which is $X_{SW\ STD}$= 7.1% c for the airfoil and $X_{SW\ STD}$= 2.7% c for the unswept wing (these data are also summarized in Table 4). The values of the average shock position and STD reported for the airfoil, are very similar to the values reported in Ref. [24] for same flow conditions, as obtained with schlieren and PIV techniques, confirming the accuracy of BOS for 2D applications.

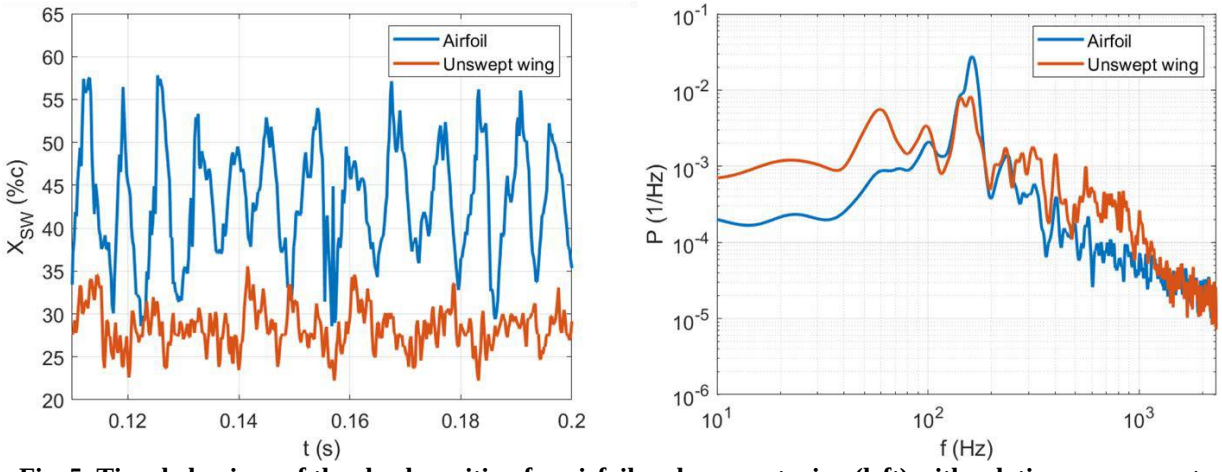

Fig. 5 Time behaviour of the shock position for airfoil and unswept wing (left) with relative power spectral density (right).

When analysing the shock position, it is evident that for the unswept wing case, the shock behaviour is less periodic, with higher frequency contributions being observable in the shockwave behavior. To complete this discussion the spectral content associated with the shock position for both the airfoil and the unswept wing is represented by its power spectral density (PSD) and shown in Fig. 5 (right). The PSD is computed with the Welch method and each PSD

is normalized by their respective variance. Both the configurations display a main peak at 160 Hz (similar to Ref. [24]). However, the general behaviour of the PSD greatly differs for the two models, with the airfoil configuration having only minor contributions at frequencies other than 160 Hz, in contrast to the unswept wing. For the latter, an additional peak, associated with the structural vibration of the wing, occurs at 60 Hz. Although for frequencies above 1050 Hz there is a good agreement between the two PSDs, the frequency contributions between 500 and 1050 Hz are more relevant for the unswept wing. These frequencies correspond to Strouhal numbers St=0.18-0.4, which are in the same broadband range of St that is often associated with the transonic buffet behavior of a swept wing [26]. This observation suggests that the buffet phenomenon is highly influenced by finite wing effects and clamping conditions.

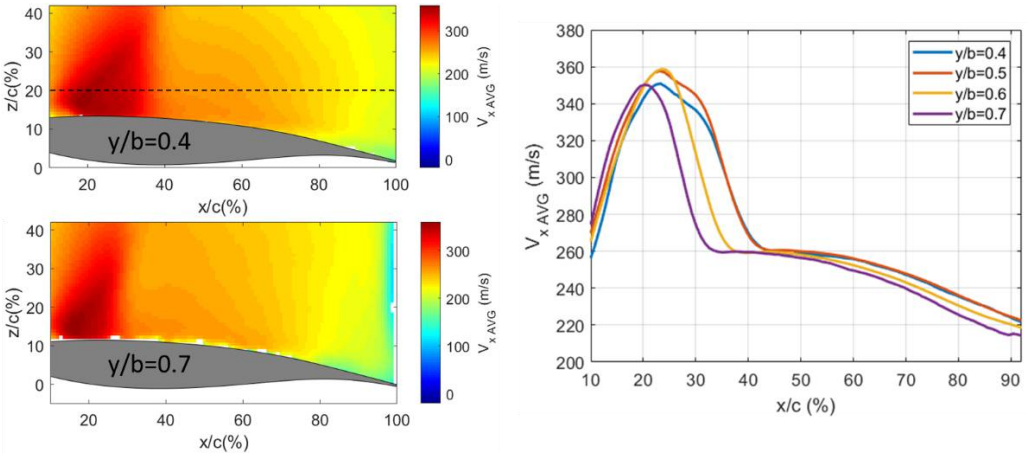

Fig. 6 Average streamwise velocity component (V_x) for the Λ=0° wing for y/b=0.4 and y/b=0.7 (left). On the right, comparison of average velocity profiles for z/c=0.2 and for y/b=(0.4, 0.5, 0.6, 0.7).

B. Flow field analysis for the unswept wing

To better address the clamping condition effects, the PIV measurements carried out for the unswept wing at different spanwise positions (y/b=0.4; 0.5; 0.6; 0.7) are discussed. For this purpose the average velocity field is shown in Fig. 6 (left) for the two most extreme measurement planes (y/b=0.4 and y/b=0.7). The comparison shows that in the most inboard section, the supersonic area encompasses a much wider region than for the plane of measurement in the neighborhood of the tip of the unswept wing. To better compare the average horizontal velocity fields, in Fig. 6 (right) the velocity profiles for z/c=0.2 and for 0.1<x/c<0.95 (corresponding to the dashed line in Fig. 6, left) are shown for all four measurement planes. The plot confirms an upstream shift of the average terminating shock position when moving from the most inboard test location to the most outboard. In addition, for the most outboard location, a further reduction of the velocity is observed for 0.5<x/c<0.95. Very similar results are obtained for y/b=0.4 and y/b=0.5 both in terms of shockwave position and velocity development downstream of the shockwave.

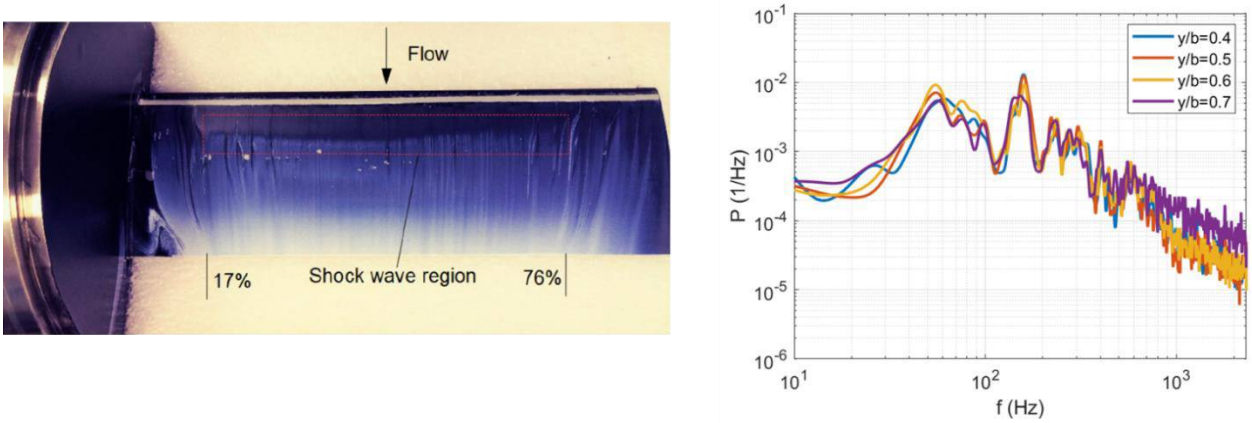

Fig. 7 Oil flow visualization of unswept wing at Ma=0.7, α=3.5° (left). Power spectral density of SW position tracked in the four different measurement planes (right).

These observations are in good agreement with an oil flow visualization performed on the same model and flow conditions (Fig. 7, left) where the most downstream shockwave position is observed between 0.4<y/b<0.5. In addition the presence of both wing root and wing tip interaction is noted.
The shockwave has been tracked using the PIV data by monitoring the gradient of the horizontal velocity component. The computed values of average shock position and standard deviation are reported in Table 4. The results confirm the observations from Fig. 6, with more downstream shockwave positions being present for y/b=0.4 and y/b=0.5, where the widest range of oscillation of the shockwave are also achieved. By comparing the shockwave properties of the unswept wing computed with both BOS and PIV, it is evident that the BOS data are closer to the range of values observed for the most outboard PIV planes of measurement.
The power spectral density associated with the shockwave position in the different measurement planes have been plotted in Fig. 7 (right). The different spectra are practically overlapping over the entire spectrum, except for the most outboard location (y/b=0.7).
Comparing the spectral analysis in Fig. 7 (right), based on the PIV data, with the plot of Fig. 5 (right), based on the BOS data, a very good match between the two techniques is achieved. This confirms that BOS is able to characterize the main features of buffet on an unswept wing, although not being capable to characterize the flow features at different spanwise locations.

Table 4 Average and standard deviation of shockwave position for different configurations.

Configuration	SW_{AVG} (%c)	SW_{STD} (%c)
BOS, Airfoil	42.8	7.1
BOS, Λ=0° wing	28.3	2.7
PIV, Λ=0° wing, y/b=0.4	35.3	3.5
PIV, Λ=0° wing, y/b=0.5	35.2	3.3
PIV, Λ=0° wing, y/b=0.6	30.5	2.8
PIV, Λ=0° wing, y/b=0.7	27.7	2.4

IV.Effect of sweep angle

A. Instantaneous flow field

To describe the behavior of transonic buffet in presence of sweep angle, the instantaneous Mach number field (computed from the velocity data with the assumption of constant total temperature) is discussed for one entire buffet cycle for the Λ=30° wing. To analyze the cycle, 6 snapshots with a time separation of 3Δt (i.e. 0.645 ms; with Δt=0.215 ms being the time interval between subsequent acquisitions) are taken into consideration (see Fig. 8).

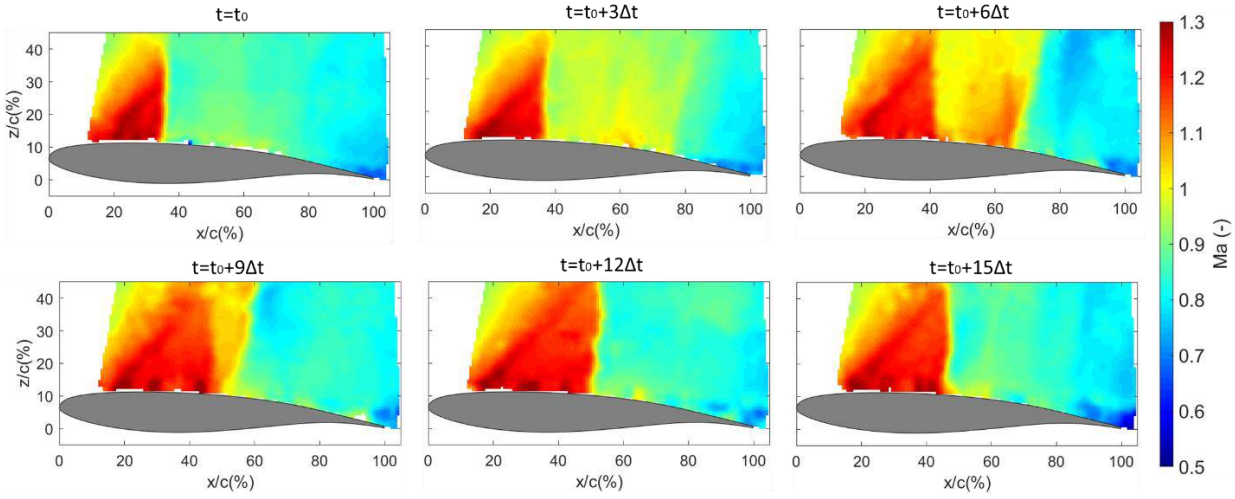

Fig. 8 Instantaneous visualization of the Mach number field in 6 different time steps for the Λ=30° wing.

In the first time step (t_0) the shockwave is located in its most upstream position (x/c=0.35). In the following image ($t=t_0+3\Delta t$), the shockwave moves downstream and a region of accelerated flow is observed for 0.4<x/c<0.7. In the

following time step (image in the top right) this region has become locally supersonic and a secondary shockwave structure appears at x/c=0.65. In the figure in the bottom left the main shockwave structure has moved downstream, while the secondary shockwave is moving upstream. As a result of the opposite motion of the two shockwave structures, they are observed to merge in the $t=t_0+12\Delta t$ image, with a primary shockwave structure reaching its most downstream position (x/c=0.5). In the following time step the shockwave starts again its upstream movement. A similar description of secondary supersonic areas can be found in Ref. [30] for a similar range of flow conditions (although for non-buffet conditions) and is attributed to the curvature of the airfoil.

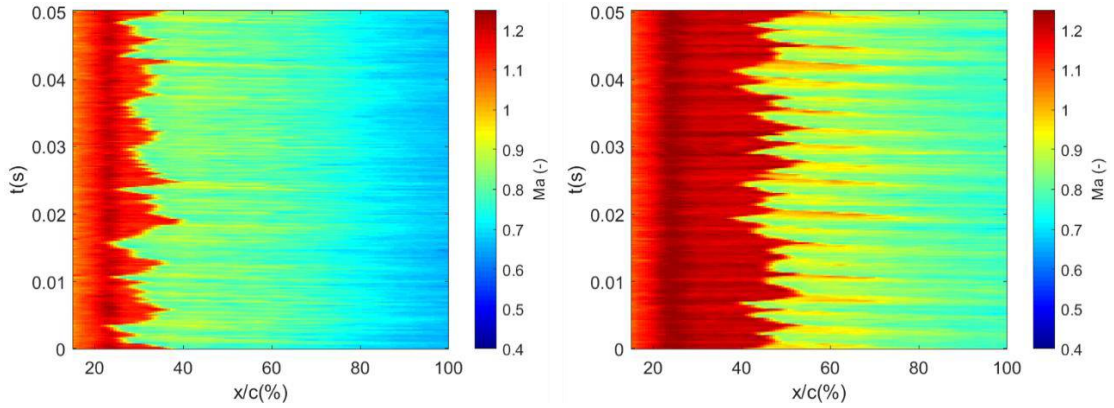

Fig. 9 Mach number profile for y/b=0.6 and z/c=0.2, for the Λ=15° (left) and the Λ=30° wings (right).

To characterize the time evolution of the Mach field for a larger interval, the profile of the Mach number field for y/b=0.6 and z/c=0.2 is shown in Fig. 9 for the Λ=15° and the Λ=30° wings. The Mach number profile of the latter (Fig. 9 right) clearly reveals the oscillation of the primary shockwave structure (between 40 and 55% c) and the intermittent presence of a secondary supersonic area, which extends approximately until 80% c. As shown from the instantaneous images in Fig. 8, the secondary supersonic area is formed during the second half of the downstream travel of the primary shockwave and disappears when this shock reaches its most downstream position.
Differently, the time evolution of the profile of the Λ=15° wing (Fig. 9 left) shows a more upstream shockwave location (between 25 and 35% c) with only subsonic expansions of the flow downstream of the supersonic area.

B. Averaged velocity fields

In Fig. 10 the time-average velocity fields for each of the three components (oriented along the x, y and z axis, as defined in Fig. 1, right) is shown for the Λ =30° swept wing for y/b=0.6 (and with Ma=0.81 and α=3.4°). The extent of the supersonic area is quite evident from both u (streamwise velocity component, in the direction of the wind tunnel centre line) and v (velocity component along the y-axis, in the direction normal to the wind tunnel side wall).

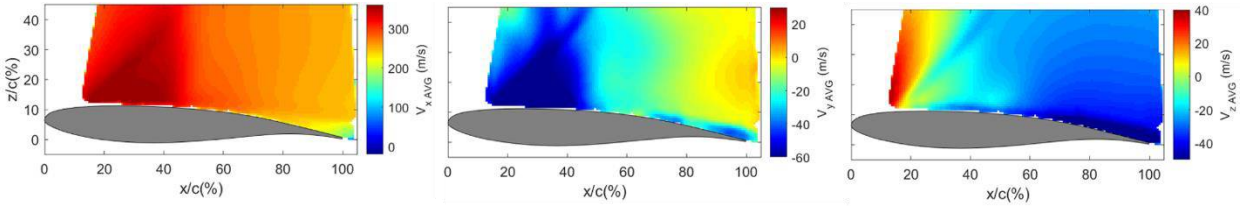

Fig. 10 Average velocity field for u (left), v (center) and w (right) for the 30° swept wing for Ma=0.81 and α=3.4° at 60% of the span.

For this configuration, at least in an average sense, no appreciable separated area can be observed, with a relevant reduction of the streamwise velocity component occurring only in proximity of the trailing edge of the wing. The vertical velocity component (w, in the direction normal to the plane of the wing) has its maximum value in the most upstream region of the FOV, due to the curvature of the airfoil. A slight increase of vertical velocity is also observed in the shockwave oscillation area, for x/c≈0.45. Regarding the out-of-plane velocity component (v), in addition to the supersonic area, a region of negative velocity is observed in the area close to the trailing edge. In the remaining portion of the FOV the variations of velocity of the out-of-plane component remain limited.

To quantify the unsteadiness present in the velocity field the standard deviations of the three velocity components are shown in Fig. 11 for the same plane of measurement (y/b=0.6). The plot clearly shows unsteadiness due to the shock oscillation for both the streamwise (left) and the out-of-plane velocity component (center) in the range 0.4<x/c<0.5. Although upstream of the shockwave the unsteadiness is very limited, additional unsteadiness (caused by the pulsating formation of the secondary supersonic region) is observed. Further fluctuations occur, for all the velocity components, in proximity of the trailing edge, suggesting the presence of an intermittent separated area. For the vertical velocity component (right), relevant oscillations are observed between 40 and 60% of the chord and are attributed to fluctuations of the shockwave position and inclination throughout the buffet cycle.

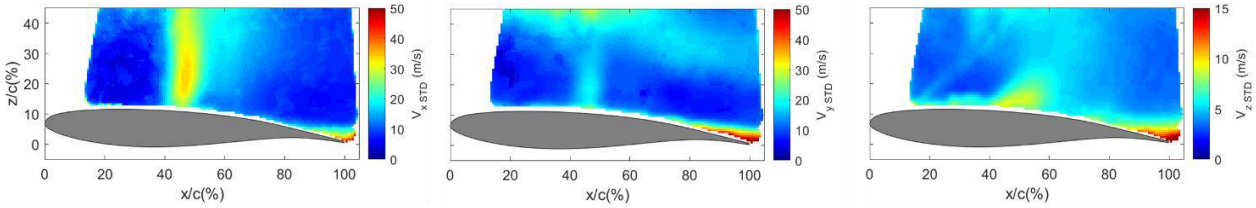

Fig. 11 Standard deviation of velocity field for u (left), v (center) and w (right) for the 30° swept wing for Ma=0.81 and α=3.4° at 60% of the span.

For brevity, for the 15° sweep angle wing only the horizontal velocity component and the corresponding standard deviation are presented (see Fig. 12). It is clear that, compared to the 30° wing, the extent of the supersonic area is much more limited, with the shockwave located more upstream (x/c≈0.3) and the relative amplitude of oscillation reduced to 10% c. No unsteadiness is present at the trailing edge of the wing, suggesting that for this configuration and flow conditions, the separated area is not even present in an intermittent fashion. No velocity fluctuations are observed downstream of the shockwave oscillation range, confirming the absence of a secondary supersonic area.

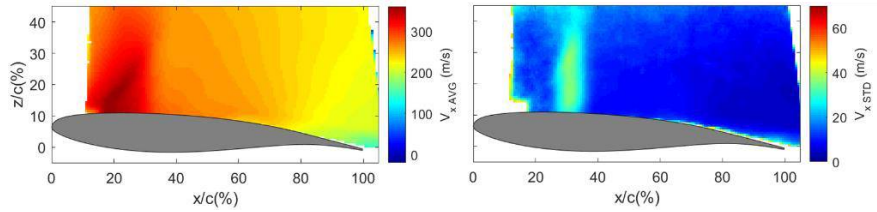

Fig. 12 Average (left) and standard deviation (right) of velocity field for the u-component of the 15° swept wing for Ma=0.72 and α=3.4° at 60% of the span.

C. Shock dynamics

To quantitatively compare the behavior of the shockwave for the different configurations, its position has been tracked in all the PIV measurement planes, as commented previously for the unswept wing in Section III.

In Fig. 13, the region of oscillation of the shock position is indicated for all the wings and for all the span locations, providing its average value and the relative standard deviation. The wing with the largest amplitude of oscillation is the Λ =30° wing, for which the values of STD are in the range 3.9-4.9% c. From the BOS images a slight underestimation of the fluctuations of the shock position is obtained for the Λ =30° wing, with $SW_{STD\text{-}BOS}$=3.8% c. The PIV data confirm that in presence of the largest sweep angle, the most downstream average shockwave positions are achieved ($0.44<X_{SW\ Avg}/c<0.47$). In contrast, for both Λ =0° and Λ =15° values close to 30% c are computed. However, it should be remembered that, although the normal Mach number is constant, the free stream Mach number differs for each of the wings. From the comparison of the range of the shockwave oscillations, it emerges that only for the unswept wing there is a relevant variation of the shockwave position along the span. This observation may be explained by the fact that in presence of sweep angle the tip vortex affects a smaller extent of the span.

From the time behaviour of the shock position, the corresponding power spectral density has been determined for all the measurement planes. To have a comparison between the spectral content of the shockwave position for the different wings, the PSD of the shock position is shown for all the wings, for the same spanwise plane y/b=0.6, in Fig 14 (left). The wings exhibit a similar spectral content, with main contributions at 60 Hz (oscillation of the model), 160 Hz (2D buffet frequency) and 400 Hz (wind tunnel contribution). In addition to these peaks additional energetic contributions are observed in the range 450-850 Hz, which, as previously commented, is in the same range of frequencies obtained in literature for 3D buffet. When comparing the different configurations it is also observed that,

with the increasing value of the sweep angle (also associated with an increase of the free stream Mach number), there is an increase in the wind tunnel contribution at 400 Hz.

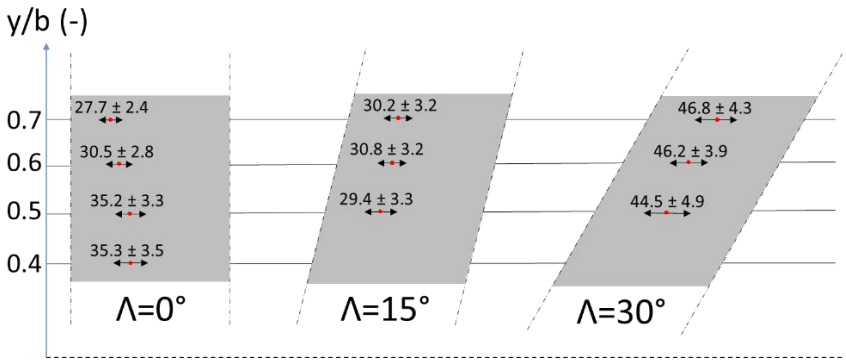

Fig. 13 Sketch of the three wings with indication of average and standard deviation of shockwave oscillation for each plane of measurement.

To verify variations in the spectral content of the shockwave oscillation along the span, the PSDs of the shockwave position are compared for the different measurement planes of the 30° sweep angle wing (see Fig. 14, right). Also in this case a similar distribution of the PSDs is observed, with no variation in the relevance of the 2D buffet peak (at 160 Hz) or in the range 450-850 Hz. However, an increase of the values of the PSDs for f>1000 Hz is observed for both y/b=0.7 and y/b=0.5, as compared to y/b=0.6.

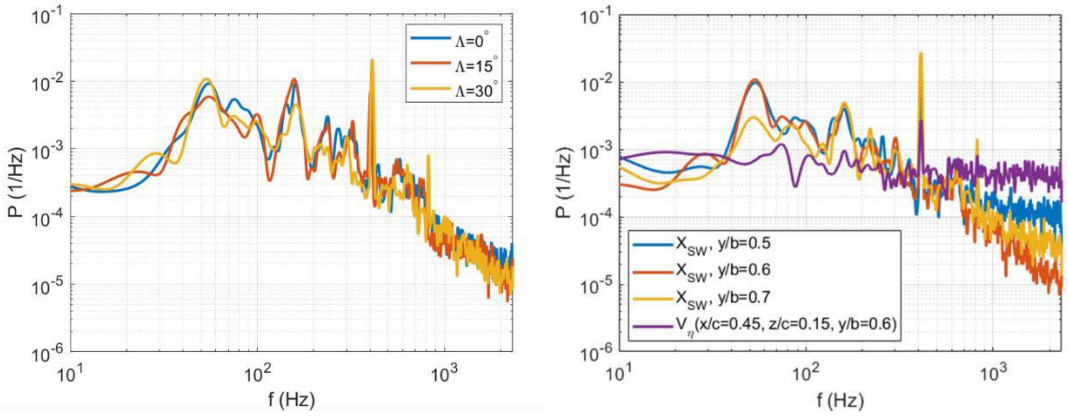

Fig. 14 Comparison of the PSD of the SW position for different wings for y/b=0.6 (left). On the right comparison of the PSD of the SW position for different measurement planes (y/b=0.5, 0.6, 0.7) for the Λ=30° wing. The purple line indicates the PSD of the spanwise velocity component in x/c=0.45, z/c=0.15, y/b=0.6 .

D. Spanwise velocity component

To analyze the spanwise behavior of the velocity field, a rotated coordinate system oriented along the leading edge of the wings (η) and in the orthogonal direction (ζ) has been adopted (see the two coordinate systems in Fig. 1, right). The velocity component orthogonal to the leading edge (V_ζ) and the one oriented along the leading edge direction of the wing (V_η) are computed as:

$$V_\zeta = V_x \cos\Lambda - V_y \sin\Lambda \quad (1)$$

$$V_\eta = V_x \sin\Lambda + V_y \cos\Lambda \quad (2)$$

With V_η being positive going from the root to the tip of the wing. In Fig. 15 the average spanwise velocity is shown for the Λ =30° wing for all the measurement planes (y/b=0.5 on the left, y/b=0.6 in the center and y/b=0.7 on the

right). In large part of the FOV there is a nearly uniform outboard velocity of approximately 120 m/s in the shockwave oscillation region and in the range from 70 to 100 m/s in the trailing edge area.
The values of the spanwise component in the trailing edge area are very close to the convection velocity obtained by Ref. [10] for the buffet cells. Differently, the value of spanwise velocity in the shockwave oscillation range is higher than the convection velocity obtained by Ref. [9,10] (where a convection velocity of approximately 60 m/s was reported).
In Fig. 14 (right) the spectral content of the time variation of the spanwise velocity component (V_η) in a point in the shockwave oscillation range is reported (x/c=0.45, z/c=0.1, y/b=0.6). No relevant contributions are observable at the 2D buffet frequency (160 Hz), while relative higher energetic contributions are present at higher frequencies.

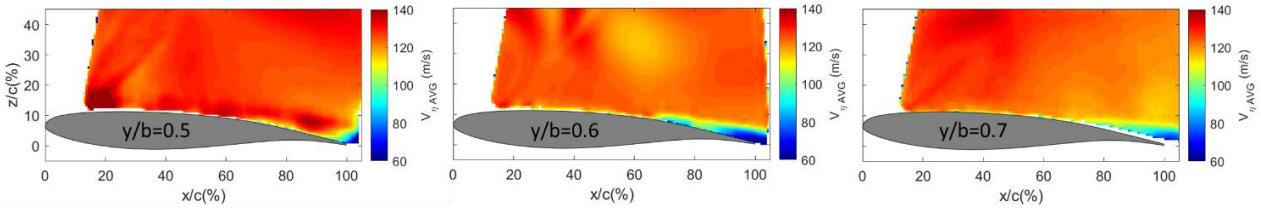

Fig. 15 Comparison of spanwise component of velocity for the Λ=30° wing for y/b=0.5 (left), y/b=0.6 (center) and y/b=0.7 (right).

V. Conclusion

In this paper transonic buffet has been studied experimentally, to investigate the effect of both the sweep angle and of the free tip of a wing. This study showed an appreciable difference in the transonic buffet behavior between a full span unswept wing (airfoil) and an unswept wing of finite span (clamped on just one side of the wind tunnel). The results clearly reveal that the buffet oscillations are more relevant and periodic in the case of the airfoil than for the unswept wing (see Fig. 5), with the shockwave located much more downstream in the former case. The use of PIV in different planes of measurement demonstrated that the shockwave is located more upstream and oscillating in a more restricted region at outboard locations (Fig. 6). These results suggest that at those locations an effect of the wing tip vortex on the buffet behavior is felt, as also supported by additional oil flow visualization. Spectral analysis showed that the presence of the free tip of the wing also gives rise to structural oscillation of the wing, which occurs at 60 Hz (Fig. 7).
The application of both BOS and PIV for the study of the unswept wing, has also validated the use of the BOS technique for analyzing transonic buffet on models with 3D structures developing along the span. From the BOS images it has been possible to obtain results in agreement with the PIV data, in particular in terms of amplitude of the shockwave oscillation. Thus, the use of the BOS technique could be applied to future studies of transonic buffet on unswept wings, especially when a qualitative visualization of the flow field is needed, or for the identification of the most developed buffet conditions, for which analysis the use of PIV could be too complicated and/or time consuming. Additional discrepancies could arise from BOS measurements on swept models in view of the additional spanwise variability of the flow field. Notwithstanding this, by orienting the BOS camera in the direction of the leading edge of the wings, a good approximation (although underestimated) of the amplitude of the shockwave is obtained.
To analyze the effect of sweep angle, the behavior of wings with different sweep angle (Λ=0°, 15° and 30°) have been compared, using for each wing the same normal Mach Number (with respect to the wing leading edge). At these flow conditions, much more downstream shockwave positions and a wider range of oscillations are achieved for the Λ=30° wing, while similar results are observed for the other two wings (see Fig. 13). For the configuration with the larger sweep angle a periodic formation of a secondary supersonic area characterizes the shockwave oscillations during the buffet cycle. An analogous behavior was not observed for the Λ=15° and the unswept wings (Fig. 9).
Evidence was found of an intermittent separated trailing edge area that occurs only for the larger sweep angle wing (Fig. 10 and Fig. 11). Near the trailing edge region of the Λ=30° wing, spanwise velocity components are found which are in the same range of the convection velocities obtained by Ref. [9,10] for the buffet cells. To better visualize the buffet cells, a PIV analysis in a measurement plane oriented along the span or with a volumetric set-up (tomographic PIV) is suggested for further studies.
A similar frequency content of the shockwave dynamics has been observed for the three wings. For all the models there is a reduction of the 2D buffet peak compared to the airfoil case, together with an increase for frequencies in the range of 450-850 Hz. Regarding the primary buffet frequency, a reduced relevance of the peak at 160 Hz has been noticed for the Λ=30° compared to the other wings. No relevant variations are instead visualized along the span of the

swept wing. The increase of frequency contributions in the range between 450 and 850 Hz is in agreement with literature, in terms of Strouhal number (St=0.18-0.4).

Although these results show some variations in the shockwave buffet oscillation in presence of an increasing sweep angle, the current findings also indicate that an aspect which could influence the comparison of the behavior of an airfoil and that of a wing is the different boundary conditions associated with the clamping of the model. Therefore, it is strongly suggested for future research, that the buffet behavior of a swept wing is always be compared with the corresponding unswept (finite-span) wing, rather than the corresponding airfoil. Similarly, the effect of the boundary conditions of an unswept wing model in transonic buffet conditions should be further investigated.

Acknowledgments

This work has been carried out as part of the project HOMER (Holistic Optical Metrology for Aero-Elastic Research), funded by the European Commission, program H2020 under Grant No. 769237.

References

[1] Hilton, W.F., and Fowler, R.G, "Photographs of Shock Wave Movement", NPL R&M No. 2692, 1947.

[2] Lee, B.H.K., "Transonic buffet on a supercritical aerofoil", *The Aeronautical Journal*, 94(935) 143-152, 1990.

[3] Jacquin, L., Molton, P., Deck, S., Maury, B., and Soulevant, D., "Experimental study of shock oscillation over a transonic supercritical profile", *AIAA Journal*, 47(9):1985–1994, 2009.

[4] Garnier, E., and Deck, S., "Large-Eddy Simulation of Transonic Buffet over a Supercritical Airfoil", In Armenio, V., Geurts, B., and Fröhlich, J., editors, *Direct and Large-Eddy Simulation VII*, 549–554, Springer Netherlands, Dordrecht, 2010.

[5] Hartmann, A., Feldhusen, A., and Schröder, W., "On the interaction of shock waves and sound waves in transonic buffet flow", *Physics of Fluids*, 25(2):026101, 2013.

[6] D'Aguanno, A., Schrijer, F.F.J., and van Oudheusden, B.W., "Spanwise organization of upstream traveling waves in transonic buffet", *Physics of Fluids*, 33:106105, 2021.

[7] Crouch, J. D., Garbaruk, A., Magidov, D., and Travin., A., "Origin of transonic buffet on aerofoils", *Journal of Fluid Mechanics*, 628:357–369, 2009.

[8] Sartor, F., Mettot, C., and Sipp, D., "Stability, receptivity, and sensitivity analyses of buffeting transonic flow over a profile", *AIAA Journal*, 53:1980–1993

[9] Paladini, E., Dandois, J., Sipp, D., and Robinet, J. "Analysis and Comparison of Transonic Buffet Phenomenon over Several Three-Dimensional Wings". *AIAA Journal*, 57. 1-18, 2018.

[10] Dandois, J., "Experimental study of transonic buffet phenomenon on a 3D swept wing", *Physics of Fluids*, 28:016101, 2016.

[11] Sugioka, Y., Numata, D., Asai, K., Koike, S., Nakakita, K., and Koga, S., "Unsteady PSP measurement of transonic buffet on a wing", *Proceedings of the 53rd AIAA Aerospace Sciences Meeting*, Vol. 1, Paper 0025, Kissimmee, January 2015.

[12] Ohmichi, Y., Ishida, T., and Hashimoto, A., "Modal Decomposition Analysis of Three-Dimensional Transonic Buffet Phenomenon on a Swept Wing," *AIAA Journal*, 56(10):3938–3950, 2018.

[13] Mayer, R., Lutz, T., Krämer, E., and Dandois, J., "Control of Transonic Buffet by Shock Control Bumps on Wing-Body Configuration", *Journal of Aircraft*, 56:1-13, 2019.

[14] Iovnovich, M., and Raveh, D.E., "Numerical Study of Shock Buffet on Three-Dimensional Wings", *AIAA Journal*, 53:449–463, 2015.

[15] Roos, F.W., "The buffeting pressure field of a high-aspect-ratio swept wing," *18th Fluid Dynamics and Plasma Dynamics and Lasers Conference*, AIAA Paper 1985-1609, July 1985.

[16] Plante, F., Dandois, J., and Laurendeau, E., "Similarities between cellular patterns occurring in transonic buffet and subsonic stall", *AIAA Journal*, 58(1):71-84, 2019.

[17] Plante, F., Dandois, J., Sartor, F., and Laurendeau, E., "Study of Three-Dimensional Transonic Buffet on Swept Wings", *35th AIAA Applied Aerodynamics Conference*, AIAA Paper 2017- 3903, Denver, June 2017.

[18] Thiery, M., and Coustols, E., "Numerical Prediction of Shock Induced Oscillations over a 2-D Airfoil: Influence of Turbulence Modelling and Test Section Walls", *International Journal of Heat and Fluid Flow*, 27(4):661–670, 2006

[19] Crouch, J., Garbaruk, A., and Strelets, M., "Global instability in the onset of transonic-wing buffet". *Journal of Fluid Mechanics*, 881, 3-22, 2019.

[20] Timme, S., "Global instability of wing shock-buffet onset", *Journal of Fluid Mechanics*, 885, 2020.

[21] Koike, S., Ueno, M., Nakakita, K., and Hashimoto, A., "Unsteady pressure measurement of transonic buffet on Nasa common research model", *AIAA Paper* No. 2016-4044, 2016.

[22] Masini, L., Timme, S., and Peace, A.J., "Analysis of a civil aircraft wing transonic shock buffet experiment," *Journal of Fluid Mechanics*, 884, 2020.

[23] Lawson, S.G., Greenwell, D., and Quinn, M., "Characterisation of Buffet on a Civil AircraftWing," *54th AIAA Aerospace Science Metting*, AIAA Paper 2016-1309, San Diego, January 2016.

[24] D'Aguanno, A., Schrijer, F.F.J., and van Oudheusden, B.W., "Experimental investigation of the transonic buffet cycle on a supercritical airfoil", *Experiments in Fluids*, 62, 214, 2021.
[25] Feldhusen-Hoffmann, A., Lagemann, C., Loosen, S., Meysonnat, P., Klaas, M., and Schröder, W., "Analysis of transonic buffet using dynamic mode decomposition", *Experiments in Fluids*, 62:66, 2021.
[26] Giannelis, N.F., Vio, G.A., and Levinski, O., "A review of recent developments in the understanding of transonic shock buffet", *Progress in Aerospace Sciences*, 92:39–84, 2017.
[27] Ragni, D., Schrijer, F.F.J., van Oudheusden, B.W., and Scarano, F., "Particle tracer response across shocks measured by PIV", *Experiments in Fluids*, 50:53–64, 2011.
[28] Sciacchitano, A., and Scarano, F., "Elimination of PIV light reflections via a temporal high pass filter", *Measurement Science and Technology*, 25(8):084009, 2014.
[29] Rajendran, L., Zhang, J., Bhattacharya, S., Bane, S., and Vlachos, P., "Uncertainty Quantification in density estimation from Background Oriented Schlieren (BOS) measurements", *Measurement Science and Technology*, 31(5):054002, 2019
[30] Kuzmin, A., "On the lambda-shock formation on ONERA M6 wing". *International Journal of Applied Engineering Research*, 9(20):7029-7038,2014.